ON SCATTERING IN DISSIMILAR PIEZOELECTRIC MATERIALS BY A SEMI-INFINITE INTERFACIAL CRACK

by ALBERT C. TO, SHAOFAN LI[†] *and* STEVEN D. GLASER

(*Department of Civil and Environmental Engineering, University of California, Berkeley, California, USA*)

[Received 24 August 2004. Revise 1 February 2005]

Summary

This work is concerned with the diffraction and scattering of plane electro-acoustic waves by an interfacial crack between two dissimilar piezoelectric half-spaces. An exact solution is obtained for the full scattering field around the tip of the interfacial crack that is loaded with both acoustic SH and electric incident waves. First, it has been found that the interfacial crack is not completely opaque to the electro-acoustic wave: the electro-acoustic wave can penetrate and transmit to the other side of the interfacial slit. Secondly, the analysis has confirmed that the interaction between electric waves and acoustic waves will provide multiple electro-acoustic head waves. Thirdly, the effects of the electro-acoustic surface wave on the scattering field have been examined. The scattering patterns obtained are fundamentally different from the prediction of the scattering theory for purely elastic media. They provide unique electro-acoustic signatures for layered piezoelectric materials.

1. Introduction

The electro-acoustic wave diffraction problem in piezoelectric and ferroelectric materials has some important applications in electronic material science, sensor technology, inverse methods, and non-destructive inspection. There has been some exploratory research on the subject, mainly from the perspective of the maintenance of smart structures (**1**, **2**). Establishing a scattering theory for interfacial defects of dissimilar piezoelectric materials will provide a solid theoretical foundation for defect inspection and probing at various length scales for structural reliability analysis.

The physics theory of electro-acoustic wave scattering in piezoelectric materials is still an open subject. This is because the fully coupled Christoffel–Maxwell equations of piezoelectric media are analytically intractable, and the simplified wave equations under the quasi-static approximation are not mathematically well-posed. In an attempt to regularize wave equations for piezoelectric media while still retaining the simplicity of the quasi-static approximation, a few regularization procedures have been proposed (**3** to **6**). These developments provide a foundation on which to establish a much needed electro-acoustic wave scattering theory for piezoelectric materials. The first systematic effort at establishing such a theory was carried out by Li (**4**). Here, we extend the electro-acoustic wave scattering theory to a medium which contains dissimilar piezoelectric phases.

We study both electric and electro-acoustic wave scattering by an interfacial crack between two dissimilar piezoelectric half-spaces subjected to both incident plane SH acoustic waves and incident

[†] ⟨li@ce.berkeley.edu⟩

Q. Jl Mech. Appl. Math. (2005) 58 (2), 309–331
doi:10.1093/qjmamj/hbi014

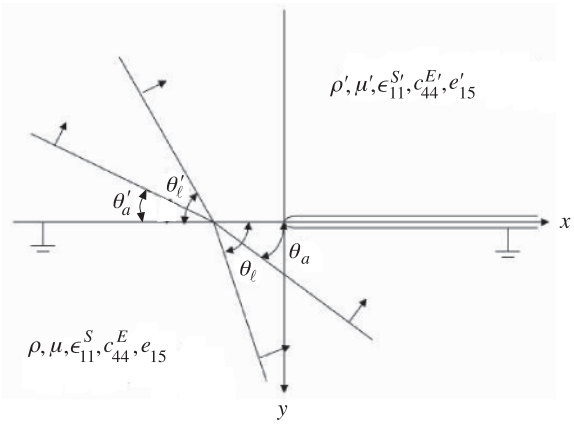

Fig. 1 Schematic illustration of a system of plane waves due to an incident acoustic wave approaching a semi-infinite crack

plane electrical waves. Conducting interfacial cracks often exist along the electrodes in multilayer piezoelectric sensors and are critical to the reliability of these devices (**7** to **9**). We are interested in the characterization of the field scattered by an interfacial crack. It may provide vital information for non-destructive inspection of these piezoelectric devices.

2. The scattering problem

2.1 *Formulation*

Consider two transversely isotropic dissimilar piezoelectric half-spaces in a Cartesian coordinate system (x, y, z), which are poled in the z-direction and share an interface located at the plane $y = 0$ (Fig. 1). For $x < 0$, the half spaces are bonded together mechanically, while no bond exists for $x \geqslant 0$. It is assumed that the interface slit is conductive, grounded, and has a vanishingly small thickness.

The material properties and the field variables in the upper half-space ($y \leqslant 0$) are labelled with a prime ($'$) while those in the lower half-space ($y > 0$) are unprimed. For the scattering problem, the relevant electromechanical coupling on the transverse plane between anti-plane displacement and in-plane electric field are

$$\mathbf{u} = \big(0, 0, w(x, y, t)\big), \quad \mathbf{E} = \left(-\frac{\partial \phi}{\partial x}, -\frac{\partial \phi}{\partial y}, 0\right). \tag{2.1}$$

Introduce a pseudo-electric potential function

$$\psi = \phi - (e_{15}/\epsilon_{11}) C_f w, \tag{2.2}$$

where $C_f = c_\ell^2/(c_\ell^2 - c_a^2)$, $c_\ell = (\epsilon_{11}\mu_0)^{-1/2}$, $c_a = \sqrt{\bar{c}_{44}/\rho}$ and $\bar{c}_{44} = c_{44}^E + {e_{15}}^2/\epsilon_{11}$.

Following Li (**10**), we then have a system of decoupled wave equations,

$$\left(\frac{\partial^2}{\partial x^2}+\frac{\partial^2}{\partial y^2}-\frac{1}{c_a^2}\frac{\partial^2}{\partial t^2}\right)w=0,\quad \left(\frac{\partial^2}{\partial x^2}+\frac{\partial^2}{\partial y^2}-\frac{1}{c_\ell^2}\frac{\partial^2}{\partial t^2}\right)\psi=0. \tag{2.3}$$

Under the quasi-hyperbolic approximation, the relevant constitutive equations are

$$\sigma_{xz}=\tilde{c}_{44}\frac{\partial w}{\partial x}+e_{15}\frac{\partial \psi}{\partial x},\ \ \sigma_{yz}=\tilde{c}_{44}\frac{\partial w}{\partial y}+e_{15}\frac{\partial \psi}{\partial y}, \tag{2.4}$$

$$D_x=e_{15}(1-C_f)\frac{\partial w}{\partial x}-\epsilon_{11}\frac{\partial \psi}{\partial x_1},\ \ D_y=e_{15}(1-C_f)\frac{\partial w}{\partial y}-\epsilon_{11}\frac{\partial \psi}{\partial x_2}, \tag{2.5}$$

where $\tilde{c}_{44}=\bar{c}_{44}[1-(1-C_f)({e_{15}}^2/\bar{c}_{44}\epsilon_{11})]$.

The 'quasi-hyperbolic' assumption has been applied to solve anti-plane transient wave propagation and scattering problems by Li (**3**, **4**); these are difficult to solve by Voigt's 'quasi-static' approximation. The quasi-static approximation assumes the speed of light to be infinite and leads to the loss of hyperbolicity of the pseudo-electric potential wave equation. The quasi-hyperbolic assumption was developed to maintain the hyperbolicity of the wave equations while simplifying the solutions: it discards the rotational electric field of the constitutive equations, but retains the finite speed of light. Recently, a similar approach called the 'electrically irrotational' approximation has been proposed: it neglects the rotational field but retains the hyperbolicity of the electro-mechanical wave equations (**5**).

A set of equations analogous to (2.1) to (2.5) holds in the upper half-space. To facilitate the presentation, we assume that the light and acoustic wave speeds are in the following order: $c_\ell > c'_\ell > c_a > c'_a$. Note that if the wave speeds are in a different order, the result may be different, but the qualitative characteristics and the procedure taken to arrive at the solution are the same.

2.2 *The scattering problem*

For time $t < 0$, an incident SH acoustic plane wave or an incident pseudo-electric wave impinges on the bonded interface and creates a system of reflected and transmitted plane waves. The incident plane waves are of the following general form:

$$w^{(i)}(x,y,t)=w_0^{(i)}G\big(t-s_a[x\cos\theta_a-y\sin\theta_a]\big),$$

$$\psi^{(i)}(x,y,t)=\psi_0^{(i)}G\big(t-s_\ell[x\cos\theta_\ell-y\sin\theta_\ell]\big),$$

where the subscripts 'a' and 'ℓ' correspond to the acoustic and pseudo-electric waves, $w_0^{(i)}$ and $\psi_0^{(i)}$ are the respective plane wave amplitudes and $s_a = 1/c_a$ and $s_\ell = 1/c_\ell$ are the respective slownesses. The angles of the incident waves are in the range $0 \leqslant \theta_a, \theta_\ell \leqslant \pi/2$. The shape function $G(\cdot)$ is a real-valued function defined to be

$$G(t)=H(t)\int_0^t g(\tau)\,d\tau,$$

where $g(\cdot)$ is a given real-valued function and $H(t)$ is the Heaviside function. For simplicity, we have assumed that the incident acoustic and pseudo-electric waves have identical shape functions.

In the case that they are different, superposition can be used to obtain the solution due to the linearity of the problem.

The incident acoustic wave impinges on the bonded interface and gives rise to the following system of reflected and transmitted plane waves:

$$w^{(r)}(x,y,t) = w_0^{(i)}\Big(\mathrm{Re}\{R_{aa}G\big(t - s_a[x\cos\theta_a + y\sin\theta_a]\big)\} - \mathcal{H}\Big\{\mathrm{Im}\{R_{aa}G\big(t - s_a[x\cos\theta_a + y\sin\theta_a]\big)\}\Big\}\Big), \tag{2.6}$$

$$w'^{(t)}(x,y,t) = w_0^{(i)}\Big(\mathrm{Re}\{T_{aa}G\big(t - s'_a[x\cos\theta'_a + y\sin\theta'_a]\big)\} - \mathcal{H}\Big\{\mathrm{Im}\{T_{aa}G\big(t - s'_a[x\cos\theta'_a + y\sin\theta'_a]\big)\}\Big\}\Big), \tag{2.7}$$

$$\psi^{(r)}(x,y,t) = w_0^{(i)}\Big(\mathrm{Re}\{R_{a\ell}G\big(t - s_\ell[x\cos\theta_\ell + y\sin\theta_\ell]\big)\} - \mathcal{H}\Big\{\mathrm{Im}\{R_{a\ell}G\big(t - s_\ell[x\cos\theta_\ell + y\sin\theta_\ell]\big)\}\Big\}\Big), \tag{2.8}$$

$$\psi'^{(t)}(x,y,t) = w_0^{(i)}\Big(\mathrm{Re}\{T_{a\ell}G\big(t - s'_\ell[x\cos\theta'_\ell + y\sin\theta'_\ell]\big)\} - \mathcal{H}\Big\{\mathrm{Im}\{T_{a\ell}G\big(t - s'_\ell[x\cos\theta'_\ell + y\sin\theta'_\ell]\big)\}\Big\}\Big). \tag{2.9}$$

Here $\mathcal{H}\{\cdot\}$ is defined as the Hilbert transform,

$$\mathcal{H}\{f(t)\} = \frac{1}{\pi}PV\int_{-\infty}^{\infty}\frac{f(\tau)}{\tau - t}\,d\tau,$$

where the Cauchy principal value of the integral is taken.

On the other hand, the incident electric wave gives rise to the following system of reflected and transmitted plane waves:

$$w^{(r)}(x,y,t) = \psi_0^{(i)}R_{\ell a}G\big(t - s_a[x\cos\theta_a + y\sin\theta_a]\big), \tag{2.10}$$

$$w'^{(t)}(x,y,t) = \psi_0^{(i)}T_{\ell a}G\big(t - s'_a[x\cos\theta'_a + y\sin\theta'_a]\big), \tag{2.11}$$

$$\psi^{(r)}(x,y,t) = \psi_0^{(i)}R_{\ell\ell}G\big(t - s_\ell[x\cos\theta_\ell + y\sin\theta_\ell]\big), \tag{2.12}$$

$$\psi'^{(t)}(x,y,t) = \psi_0^{(i)}T_{\ell\ell}G\big(t - s'_\ell[x\cos\theta'_\ell + y\sin\theta'_\ell]\big), \tag{2.13}$$

where the Rs and Ts in (2.6) to (2.13) are the reflection and transmission coefficients with the first subscript denoting the type of incident wave and the second subscript denoting the type of reflected or transmitted wave. They are given in the Appendix.

Based on Snell's law, all the plane waves have identical horizontal slowness, $s_a\cos\theta_a = s'_a\cos\theta'_a = s_\ell\cos\theta_\ell = s'_\ell\cos\theta'_\ell$, from which the reflection and transmission angles are determined for the corresponding plane waves. For a transmitted or a reflected pseudo-electric wave generated from an incident acoustic wave, when $s_a\cos\theta_a > s_\ell$, $\cos\theta_\ell$ becomes greater than unity, the term $\sin\theta_\ell$ becomes imaginary and it may be denoted as $\pm i\sqrt{s_a^2\cos^2\theta_a - s_\ell^2}$. In this case, the corresponding reflection coefficient ($R_{a\ell}$) becomes complex, and the reflected wave undergoes a phase shift and propagates along the bonded interface. The Hilbert transformed part of the reflected pseudo-electric wave in (2.8) describes the inhomogeneous part of the wave (**11**, pp. 149–157). The

Hilbert transform part vanishes when $\cos\theta_\ell \leqslant 1$, and the resulting reflected wave is homogeneous, and thus has the same shape function as the incident acoustic wave. Likewise, when $s_a \cos\theta_a > s'_\ell$, $\sin\theta'_\ell$ becomes imaginary and the transmission coefficient ($T_{a\ell}$) becomes complex. The transmitted pseudo-electric wave becomes inhomogeneous and propagates along the bonded interface. On the other hand, for transmitted or reflected pesudo-electric waves generated from an incident pseudo-electric wave, they are homogeneous since it is always true that $s_\ell \cos\theta_\ell < s'_\ell < s_a < s'_a$ because we have assumed the pseudo-electric wave velocity c_ℓ the largest. As will be seen, the incident angle has an important effect on both the scattering patterns and the dynamic intensity factors.

At time $t = 0$, a system of plane waves propagating along the bonded interface arrives at the crack tip and is scattered. The total solution of the scattering problem consists of

$$\left.\begin{aligned} w &= w^{(i)} + w^{(r)} + w^{(s)} \\ \psi &= \psi^{(i)} + \psi^{(r)} + \psi^{(s)} \end{aligned}\right\} \quad \text{for } y > 0 \quad \text{and} \quad \left.\begin{aligned} w' &= w'^{(t)} + w'^{(s)} \\ \psi' &= \psi'^{(t)} + \psi'^{(s)} \end{aligned}\right\} \quad \text{for } y < 0.$$

The superscripts (i), (r) and (s) indicate the incident, reflected and scattered fields, respectively.

For scattered fields, the following initial conditions and radiation conditions are imposed:

$$\begin{aligned} w^{(s)}(x,y,t) = w'^{(s)}(x,y,t) = \dot{w}^{(s)}(x,y,t) = \dot{w}'^{(s)}(x,y,t) = 0, \quad t < 0, \\ \psi^{(s)}(x,y,t) = \psi'^{(s)}(x,y,t) = \dot{\psi}^{(s)}(x,y,t) = \dot{\psi}'^{(s)}(x,y,t) = 0, \quad t < 0, \end{aligned}$$

where the overdot denotes $\partial/\partial t$, and

$$\lim_{r\to\infty}\left[w^{(s)}, w'^{(s)}, \psi^{(s)}, \psi'^{(s)}, \dot{w}^{(s)}, \dot{w}'^{(s)}, \dot{\psi}^{(s)}, \dot{\psi}'^{(s)}\right] = 0, \quad t > 0.$$

The mechanical and electrical boundary conditions are $\sigma_{yz}(x,0,t) = \sigma'_{yz}(x,0,t) = 0$ for $x \geqslant 0$, $w(x,0,t) = w'(x,0,t)$ for $x < 0$, and $\phi(x,0,t) = \phi'(x,0,t) = 0$ for $-\infty < x < \infty$. Consideration of these leads to the following boundary conditions for the scattered waves:

$$\sigma^{(s)}_{yz}(x,0,t) = \sigma'^{(s)}_{yz}(x,0,t) = -\sigma'^{(t)}_{yz}(x,0,t), \quad x \geqslant 0, \tag{2.14}$$

$$w^{(s)}(x,0,t) = w'^{(s)}(x,0,t), \quad x < 0, \tag{2.15}$$

$$\phi^{(s)}(x,0,t) = \phi'^{(s)}(x,0,t) = 0, \quad -\infty < x < \infty. \tag{2.16}$$

In the rest of the paper, the supersript (s) is dropped for brevity.

3. Integral equation solutions

3.1 *Transform methods*

In this section, the standard procedure of multiple Laplace transforms is employed to find the solution of the above mixed initial boundary value problem (IBVP). The multiple transforms are introduced for the variable pair (x,t). To suppress the time variable t, the usual one-sided Laplace transform is applied,

$$f^*(x,y,p) = \int_0^\infty f(x,y,t)\, e^{-pt}\, dt, \qquad f(x,y,t) = \frac{1}{2\pi i}\int_{Br_1} f^*(x,y,p)\, e^{pt}\, dp,$$

where the inversion integration is taken over the usual Bromwich path.

To suppress the spatial variable x, the two-sided Laplace transform is used:

$$\hat{f}^*(\zeta, y, p) = \int_{-\infty}^{\infty} f^*(x, y, p)\, e^{-p\zeta x}\, dx, \quad f^*(x, y, p) = \frac{p}{2\pi i} \int_{Br_2} \hat{f}^*(\zeta, y, p)\, e^{p\zeta x}\, d\zeta.$$

After transformation, the governing equations (2.3) for the scattered waves become

$$\left[\frac{d^2}{dy^2} - p^2\alpha^2(\zeta)\right] \hat{w}^*(\zeta, y, p) = 0, \quad \left[\frac{d^2}{dy^2} - p^2\beta^2(\zeta^2)\right] \hat{\psi}^*(\zeta, y, p) = 0, \quad y > 0,$$

$$\left[\frac{d^2}{dy^2} - p^2\alpha'^2(\zeta)\right] \hat{w}'^*(\zeta, y, p) = 0, \quad \left[\frac{d^2}{dy^2} - p^2\beta'^2(\zeta)\right] \hat{\psi}'^*(\zeta, y, p) = 0, \quad y < 0,$$

where $\alpha(\zeta) = \sqrt{s_a^2 - \zeta^2}$, $\beta(\zeta) = \sqrt{s_\ell^2 - \zeta^2}$, $\alpha'(\zeta) = \sqrt{s_a'^2 - \zeta^2}$ and $\beta'(\zeta) = \sqrt{s_\ell'^2 - \zeta^2}$.

To satisfy the boundary conditions at infinity, we choose the solution as follows:

$$\hat{w}^*(\zeta, y, p) = p^{-2} A(\zeta)\, e^{-p\alpha y}, \quad \hat{\psi}^*(\zeta, y, p) = p^{-2} B(\zeta)\, e^{-p\beta y}, \ y > 0, \tag{3.1}$$

$$\hat{w}'^*(\zeta, y, p) = -p^{-2} A'(\zeta)\, e^{p\alpha' y}, \quad \hat{\psi}'^*(\zeta, y, p) = -p^{-2} B'(\zeta)\, e^{p\beta' y}, \ y < 0. \tag{3.2}$$

The transformed electrical boundary condition (2.16) is

$$\hat{\phi}^*(\zeta, 0, p) = (e_{15}/\epsilon_{11}) C_f\, \hat{w}^*(\zeta, 0, p) + \hat{\psi}^*(\zeta, 0, p) = 0, \tag{3.3}$$

$$\hat{\phi}'^*(\zeta, 0, p) = (e_{15}'/\epsilon_{11}') C_f'\, \hat{w}'^*(\zeta, 0, p) + \hat{\psi}'^*(\zeta, 0, p) = 0. \tag{3.4}$$

Substituting the solutions (3.1) and (3.2) into (3.3) and (3.4), one finds that

$$B(\zeta) = -(e_{15}/\epsilon_{11}) C_f\, A(\zeta) \quad \text{and} \quad B'(\zeta) = -(e_{15}'/\epsilon_{11}') C_f'\, A'(\zeta). \tag{3.5}$$

Therefore, the displacement and the pseudo-electric potential can be expressed in terms of two unknown functions, $A(\zeta)$ and $A'(\zeta)$.

3.2 *The Wiener–Hopf decomposition*

A powerful technique to find the solution of the above IBVP in transformed space is the Wiener–Hopf decomposition. In order to apply this technique, it is expedient to first expand the mechanical boundary conditions over the full range of the x-axis. This can be done by introducing two unknown functions:

$$\sigma_-(x, t) = \begin{cases} \sigma_{yz}(x, 0, t) = \sigma_{yz}'(x, 0, t), & x < 0, \\ 0, & x \geqslant 0, \end{cases} \tag{3.6}$$

$$\Delta w_+(x, t) = \begin{cases} 0, & x < 0, \\ w(x, 0, t) - w'(x, 0, t), & x \geqslant 0, \end{cases} \tag{3.7}$$

such that

$$\sigma_{yz}(x, 0, t) = \sigma_{yz}'(x, 0, t) = \sigma_-(x, t) - \sigma_{yz}^{\prime(t)}(x, 0, t), \quad -\infty < x < \infty,$$

$$w(x, 0, t) - w'(x, 0, t) = \Delta w_+(x, t), \quad -\infty < x < \infty.$$

After suppressing both x and t,

$$\hat{\sigma}^*_{yz}(\zeta, 0, p) = \hat{\sigma}'^*_{yz}(\zeta, 0, p) = p^{-1}\Sigma_-(\zeta) - \hat{\sigma}'^{*(t)}_{yz}(\zeta, 0, p), \tag{3.8}$$

$$\hat{w}^*(\zeta, 0, p) - \hat{w}'^*(\zeta, 0, p) = p^{-2}\Delta U_+(\zeta), \tag{3.9}$$

where

$$\Sigma_-(\zeta) = p\int_{-\infty}^{0} \sigma^*_-(x, p)\, e^{-p\zeta x}\, dx, \quad \Delta U_+(\zeta) = p^2 \int_0^{\infty} \Delta w^*_+(x, p)\, e^{-p\zeta x}\, dx.$$

On the other hand, substituting (3.1), (3.2) and (3.5) into the transformed constitutive equations for the stresses σ_{yz} and σ'_{yz} in (2.4), one obtains

$$A(\zeta) = -\frac{p}{D(\zeta)}\hat{\sigma}^*_{yz}(\zeta, 0, p) \quad \text{and} \quad A'(\zeta) = -\frac{p}{D'(\zeta)}\hat{\sigma}'^*_{yz}(\zeta, 0, p), \tag{3.10}$$

where $D(\zeta) = \tilde{c}_{44}(\alpha(\zeta) - \tilde{k}_e^2\beta(\zeta))$ and $D'(\zeta) = \tilde{c}'_{44}(\alpha'(\zeta) - \tilde{k}'^2_e\beta'(\zeta))$ are recognized as the Bleustein–Gulyaev wave functions (**12** to **14**) for the lower and upper piezoelectric half spaces respectively; $\tilde{k}_e^2$ and $\tilde{k}'^2_e$ are the electro-mechanical coupling coefficients,

$$\tilde{k}_e^2 = \frac{e_{15}^2}{\epsilon_{11}\tilde{c}_{44}}C_f \quad \text{and} \quad \tilde{k}'^2_e = \frac{e'^{\,2}_{15}}{\epsilon'_{11}\tilde{c}'_{44}}C'_f.$$

Substituting (3.1), (3.2) and (3.10) into (3.9) leads to the standard Wiener–Hopf equation,

$$\Sigma_-(\zeta) - p\hat{\sigma}'^{*(t)}_{yz}(\zeta, 0, p) = K(\zeta)\Delta U_+(\zeta) \tag{3.11}$$

with

$$K(\zeta) = -\frac{D(\zeta)D'(\zeta)}{M(\zeta)}, \tag{3.12}$$

where $M(\zeta) = D(\zeta) + D'(\zeta)$ is recognized as the Maerfeld–Tournois wave function (**15**).

The term $\hat{\sigma}'^{*(t)}_{yz}(\zeta, 0, p)$ in (3.11) is dependent on the type of incident wave. Substituting the transmitted acoustic wave field and pseudo-electric wave field in (2.7) to (2.13) into the constitutive equation for stress in (2.4) and transforming, one may obtain the transmitted stress for an incident acoustic wave,

$$\hat{\sigma}'^{*(t)}_{yz}(\zeta, 0, p) = -\frac{\sigma_0 g^*(p)}{p(\zeta + s_h)}, \tag{3.13}$$

where

$$\sigma_0 = -(\tilde{c}'_{44}T_{aa}s'_a \sin\theta'_a + e'_{15}T_{a\ell}s'_\ell \sin\theta'_\ell)w_0^{(i)} \quad \text{and} \quad s_h = s_a \cos\theta_a$$

for an incident acoustic wave $w^{(i)}$, whereas

$$\sigma_0 = -(\tilde{c}'_{44}T_{\ell a}s'_a \sin\theta'_a + e'_{15}T_{\ell\ell}s'_\ell \sin\theta'_\ell)\psi_0^{(i)} \quad \text{and} \quad s_h = s_\ell \cos\theta_\ell$$

for an incident pseudo-electric wave $\psi^{(i)}$. The term in (3.13) can be reduced to the transmitted stress for the purely elastic case derived in (**16**).

The key to solving the Wiener–Hopf equation (3.11) is to factorize $K(\zeta)$ into sectionally analytic functions in the left and right half complex-ζ planes respectively. It is easier to factorize $D(\zeta)$, $D'(\zeta)$ and $M(\zeta)$ in $K(\zeta)$ separately instead of factorizing $K(\zeta)$ altogether in one step.

Define the Bleustein–Gulyaev wave speeds for the lower and upper half-spaces by

$$c_{bg} = c_a\sqrt{\tilde{C}_f(1-\tilde{k}_e^4)} \quad \text{and} \quad c'_{bg} = c'_a\sqrt{\tilde{C}'_f(1-\tilde{k}_e'^4)},$$

respectively, where

$$\tilde{C}_f = c_\ell^2/(c_\ell^2 - \tilde{k}_e^4 c_a^2) \quad \text{and} \quad \tilde{C}'_f = c_\ell'^2/(c_\ell'^2 - \tilde{k}_e'^4 c_a'^2);$$

the corresponding slownesses are $s_{bg} = 1/c_{bg}$ and $s'_{bg} = 1/c'_{bg}$.

The product decomposition of D is given in (**3**, **14**):

$$D(\zeta) = \frac{(s_{bg}+\zeta)(s_{bg}-\zeta)}{\sqrt{(s_a+\zeta)(s_a-\zeta)}}\mathcal{T}_+(\zeta)\mathcal{T}_-(\zeta)D_s, \tag{3.14}$$

$$D'(\zeta) = \frac{(s'_{bg}+\zeta)(s'_{bg}-\zeta)}{\sqrt{(s'_a+\zeta)(s'_a-\zeta)}}\mathcal{T}'_+(\zeta)\mathcal{T}'_-(\zeta)D'_s, \tag{3.15}$$

where $D_s = \tilde{c}_{44}(1-\tilde{k}_e^2)$, $D'_s = \tilde{c}'_{44}(1-\tilde{k}_e'^2)$,

$$\mathcal{T}_\pm(\zeta) = \exp\left\{-\frac{1}{\pi}\int_{s_\ell}^{s_a}\frac{\arctan(\Xi(\eta))}{\eta\pm\zeta}\,d\eta\right\}, \quad \mathcal{T}'_\pm(\zeta) = \exp\left\{-\frac{1}{\pi}\int_{s'_\ell}^{s'_a}\frac{\arctan\left(\Xi'(\eta)\right)}{\eta\pm\zeta}\,d\eta\right\},$$

$$\Xi(\eta) = -\frac{\tilde{k}_e^2\bar{\beta}(\eta)}{\alpha(\eta)}, \quad \Xi'(\eta) = -\frac{\tilde{k}_e'^2\bar{\beta}'(\eta)}{\alpha'(\eta)},$$

$\bar{\beta}(\eta) = \sqrt{\eta^2 - s_\ell^2}$ and $\bar{\beta}'(\eta) = \sqrt{\eta^2 - s_\ell'^2}$.

The function $M(\zeta)$ can be factorized as products of sectionally analytic functions,

$$M(\zeta) = \frac{(s+\zeta)(s-\zeta)}{\sqrt{(s'_a+\zeta)(s'_a-\zeta)}}(D_s+D'_s)\mathcal{S}_+(\zeta)\mathcal{S}_-(\zeta), \tag{3.16}$$

where

$$s = \begin{cases} s_{mt} & \text{if the Maerfeld–Tournois wave exists,} \\ s'_a & \text{otherwise,} \end{cases}$$

$$\mathcal{S}_\pm(\zeta) = \exp\left\{-\frac{1}{\pi}\left[\int_{s_\ell}^{s'_\ell}\frac{\arctan[\Xi_1(\eta)]}{\eta\pm\zeta}\,d\eta + \int_{s'_\ell}^{s_a}\frac{\arctan[\Xi_2(\eta)]}{\eta\pm\zeta}\,d\eta + \int_{s_a}^{s'_a}\frac{\arctan[\Xi_3(\eta)]}{\eta\pm\zeta}\,d\eta\right]\right\},$$

$$\Xi_1(\zeta) = \frac{-\tilde{k}_e^2\tilde{c}_{44}\bar{\beta}(\zeta)}{\tilde{c}_{44}\alpha(\zeta) + \tilde{c}'_{44}\alpha'(\zeta) - \tilde{k}_e'^2\tilde{c}'_{44}\beta'(\zeta)}, \quad \Xi_2(\zeta) = \frac{-\tilde{k}_e^2\tilde{c}_{44}\bar{\beta}(\zeta) - \tilde{k}_e'^2\tilde{c}'_{44}\bar{\beta}'(\zeta)}{\tilde{c}_{44}\alpha(\zeta) + \tilde{c}'_{44}\alpha'(\zeta)},$$

$$\Xi_3(\zeta) = \frac{-\tilde{k}_e^2\tilde{c}_{44}\bar{\beta}(\zeta) - \tilde{k}_e'^2\tilde{c}'_{44}\bar{\beta}'(\zeta) + \tilde{c}_{44}\bar{\alpha}(\zeta)}{\tilde{c}'_{44}\alpha'(\zeta)}, \quad \bar{\alpha}(\zeta) = \sqrt{\zeta^2 - s_a^2},\ \bar{\beta}(\zeta) = \sqrt{\zeta^2 - s_\ell^2}$$

and

$$\bar{\beta}'(\zeta) = \sqrt{\zeta^2 - s_\ell'^2}.$$

After obtaining the product decomposition above, the Wiener–Hopf equation (3.11) is solved following the procedure in (**17**). The results are

$$\Sigma_-(\zeta) = \frac{\sigma_0 g^*(p)}{\zeta + s_h}\left(\frac{R_-(-s_h)}{R_-(\zeta)} - 1\right), \tag{3.17}$$

$$\Delta U_+(\zeta) = -\frac{\sigma_0 g^*(p)(s+\zeta)\sqrt{s_a+\zeta}\,R_-(-s_h)}{(\zeta+s_h)(s_{bg}+\zeta)(s'_{bg}+\zeta)Q_s F_+(\zeta)}, \tag{3.18}$$

where

$$R_-(\zeta) = \frac{1}{F_-(\zeta)}\frac{(s-\zeta)\sqrt{s_a-\zeta}}{(s_{bg}-\zeta)(s'_{bg}-\zeta)} \quad \text{and} \quad F_-(\zeta) = \frac{\mathcal{T}_-(\zeta)\mathcal{T}'_-(\zeta)}{\mathcal{S}_-(\zeta)}. \tag{3.19}$$

Substituting (3.9), (3.10), (3.17) and (3.18) into (3.1) and (3.2), one obtains the scattered displacement and pseudo-electric wave fields:

$$w^*(x,y,p) = -\frac{\sigma_0 g^*(p)}{2\pi i p}\int_{\zeta_\alpha - i\infty}^{\zeta_\alpha + i\infty} \frac{(s+s_h)\sqrt{s_a+s_h}}{\tilde{c}_{44}(\alpha(\zeta)-\tilde{k}_e^2\beta(\zeta))(\zeta+s_h)(s_{bg}+s_h)} \times \frac{(s_{bg}-\zeta)(s'_{bg}-\zeta)}{(s-\zeta)\sqrt{(s'_{bg}+s_h)(s_a-\zeta)}}\frac{F_-(\zeta)}{F_-(-s_h)}\,e^{-p(\alpha y-\zeta x)}\,d\zeta, \tag{3.20}$$

$$\psi^*(x,y,p) = \frac{\sigma_0 g^*(p)}{2\pi i p}\frac{e_{15}C_f}{\epsilon_{11}}\int_{\zeta_\beta - i\infty}^{\zeta_\beta + i\infty} \frac{(s+s_h)\sqrt{s_a+s_h}}{\tilde{c}_{44}(\alpha(\zeta)-\tilde{k}_e^2\beta(\zeta))(\zeta+s_h)(s_{bg}+s_h)} \times \frac{(s_{bg}-\zeta)(s'_{bg}-\zeta)}{(s'_{bg}+s_h)(s-\zeta)\sqrt{s_a-\zeta}}\frac{F_-(\zeta)}{F_-(-s_h)}\,e^{-p(\beta y-\zeta x)}\,d\zeta, \tag{3.21}$$

$$w'^*(x,y,p) = \frac{\sigma_0 g^*(p)}{2\pi i p}\int_{\zeta_{\alpha'} - i\infty}^{\zeta_{\alpha'} + i\infty} \frac{(s+s_h)\sqrt{s_a+s_h}}{\tilde{c}_{44}(\alpha'(\zeta)-\tilde{k}_e^2\beta'(\zeta))(\zeta+s_h)(s_{bg}+s_h)} \times \frac{(s_{bg}-\zeta)(s'_{bg}-\zeta)}{(s'_{bg}+s_h)(s-\zeta)\sqrt{s_a-\zeta}}\frac{F_-(\zeta)}{F_-(-s_h)}\,e^{-p(-\alpha' y-\zeta x)}\,d\zeta, \tag{3.22}$$

$$\psi'^*(x,y,p) = -\frac{\sigma_0 g^*(p)}{2\pi i p}\frac{e'_{15}C'_f}{\epsilon'_{11}}\int_{\zeta_{\beta'} - i\infty}^{\zeta_{\beta'} + i\infty} \frac{(s+s_h)\sqrt{s_a+s_h}}{\tilde{c}_{44}(\alpha'(\zeta)-\tilde{k}_e^2\beta'(\zeta))(\zeta+s_h)(s'_{bg}+s_h)} \times \frac{(s_{bg}-\zeta)(s'_{bg}-\zeta)}{(s_{bg}+s_h)(s-\zeta)\sqrt{s_a-\zeta}}\frac{F_-(\zeta)}{F_-(-s_h)}\,e^{-p(-\beta' y-\zeta x)}\,d\zeta. \tag{3.23}$$

4. The Cagniard–de Hoop inversion

Having carried out the Wiener–Hopf decomposition, we are now in a position to invert the integrals in (3.20) to (3.23) to obtain explicit solutions in the physical domain. Exact inversion can be achieved by the Cagniard–de Hoop scheme (**18**, **19**). First, the scattered displacement and the pseudo-electric potential fields for an incident acoustic wave are considered so that $s_h = s_a \cos\theta_a$ in the integrals. We proceed by replacing the original Bromwich path by a deformed Cagniard contour such that the one-sided Laplace transform can be obtained by inspection.

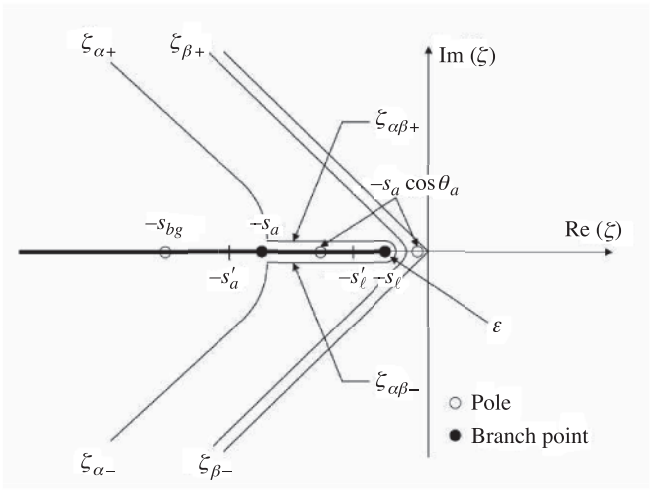

Fig. 2 Cagniard–de Hoop inversion paths Γ_α, Γ_β and $\Gamma_{\alpha\beta}$ for acoustic excitation

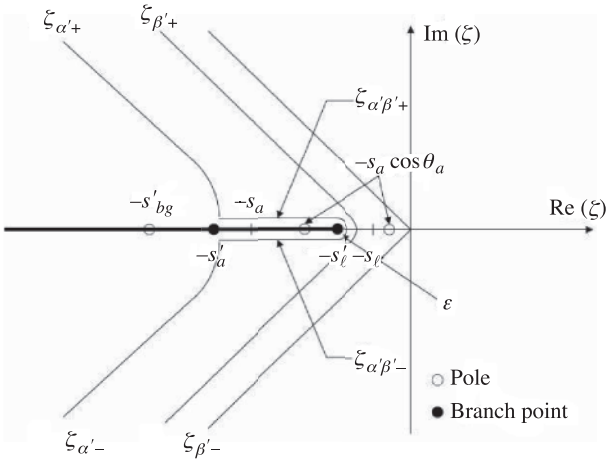

Fig. 3 Cagniard–de Hoop inversion paths $\Gamma_{\alpha'}$, $\Gamma_{\beta'}$ and $\Gamma_{\alpha'\beta'}$ for acoustic excitation

Shown in Figs 2 and 3, the following inversion paths are chosen: Γ_α, $\Gamma_{\alpha\beta}$, Γ_β, $\Gamma_{\alpha'}$, $\Gamma_{\alpha'\beta'}$ and $\Gamma_{\beta'}$ in which

$$\alpha(\zeta)y - \zeta x = t, \quad \zeta \in \Gamma_\alpha, \Gamma_{\alpha\beta}; \ \beta(\zeta)y - \zeta x = t, \quad \zeta \in \Gamma_\beta;$$
$$-\alpha'(\zeta)y - \zeta x = t, \quad \zeta \in \Gamma_{\alpha'}, \Gamma_{\alpha'\beta'}; \ -\beta'(\zeta)y - \zeta x = t, \quad \zeta \in \Gamma_{\beta'}.$$

It is more convenient to work in polar coordinates by letting $x = r\cos\theta$ and $y = r\sin\theta$. Note that at $\zeta = -s_a\cos\theta$, the path Γ_α intercepts the real axis $\mathrm{Re}(\zeta)$. Thus, a supplemental path $\Gamma_{\alpha\beta}$ is needed to circumvent the branch cut of multivalued function $\beta(\zeta) = \sqrt{s_\ell^2 - \zeta^2}$. This leads to the occurrence of the electro-acoustic head wave (see discussions in (**3**, **20**)). Along the path $\Gamma_{\alpha\beta}$, the parameter θ varies in the range

$$0 \geqslant \theta \geqslant -\theta_{\mathrm{cr}}^{a\ell} \quad \text{with} \quad \theta_{\mathrm{cr}}^{a\ell} = |\cos^{-1}(s_\ell/s_a)|.$$

Similarly, the supplemental path $\Gamma_{\alpha'\beta'}$ is added to circumvent the branch cut of $\beta'(\zeta)$. Along path $\Gamma_{\alpha'\beta'}$, the parameter θ varies in the range

$$0 \leqslant \theta \leqslant \theta_{\mathrm{cr}}^{\prime a\ell} \quad \text{with} \quad \theta_{\mathrm{cr}}^{\prime a\ell} = |\cos^{-1}(s'_\ell/s'_a)|.$$

Following de Hoop (**19**), exact inversions are found,

$$\begin{aligned}
w(x,y,t) &= \int_0^t [\mathrm{Re}(\sigma_0)G(t-\tau) - \mathrm{Im}(\sigma_0)\mathcal{H}\{G(t-\tau)\}]w_\delta(x,y,\tau)\,d\tau + w_r(x,y,t),\\
\psi(x,y,t) &= \int_0^t [\mathrm{Re}(\sigma_0)G(t-\tau) - \mathrm{Im}(\sigma_0)\mathcal{H}\{G(t-\tau)\}]\psi_\delta(x,y,\tau)\,d\tau + \psi_r(x,y,t),\\
w'(x,y,t) &= \int_0^t [\mathrm{Re}(\sigma_0)G(t-\tau) - \mathrm{Im}(\sigma_0)\mathcal{H}\{G(t-\tau)\}]w'_\delta(x,y,\tau)\,d\tau + w'_r(x,y,t),\\
\psi'(x,y,t) &= \int_0^t [\mathrm{Re}(\sigma_0)G(t-\tau) - \mathrm{Im}(\sigma_0)\mathcal{H}\{G(t-\tau)\}]\psi'_\delta(x,y,\tau)\,d\tau + \psi'_r(x,y,t),
\end{aligned}$$

where the subscript δ represents the scattering fields due to the impulsive incident wave, and w_r, ψ_r are reflected displacement and pseudo-electric fields while w'_r, ψ'_r are the refracted displacement and pseudo-electric fields. We obtain

$$\begin{aligned}
w_\delta(x,y,t) = -\frac{1}{\pi}\Bigg\{ &\mathrm{Re}\Bigg[\frac{(s+s_h)\sqrt{s_a+s_h}}{\tilde{c}_{44}(\alpha(\zeta_{\alpha+}) - \tilde{k}_e^2\beta(\zeta_{\alpha+}))(\zeta_{\alpha+}+s_h)(s_{bg}+s_h)(s'_{bg}+s_h)}\\
&\times \frac{(s_{bg}-\zeta_{\alpha+})(s'_{bg}-\zeta_{\alpha+})}{(s-\zeta_{\alpha+})\sqrt{s_a-\zeta_{\alpha+}}}\,\frac{F_-(\zeta_{\alpha+})}{F_-(-s_h)}\,\frac{\alpha(\zeta_{\alpha+})}{\sqrt{t^2-s_a^2r^2}}\Bigg]H(t-s_ar)\\
&-\mathrm{Im}\Bigg[\frac{(s+s_h)\sqrt{s_a+s_h}}{\tilde{c}_{44}(\alpha(\zeta_{\alpha\beta+}) - \tilde{k}_e^2\beta(\zeta_{\alpha\beta+}))(\zeta_{\alpha\beta+}+s_h)(s_{bg}+s_h)(s'_{bg}+s_h)}\\
&\times \frac{(s_{bg}-\zeta_{\alpha\beta+})(s'_{bg}-\zeta_{\alpha\beta+})}{(s-\zeta_{\alpha\beta+})\sqrt{s_a-\zeta_{\alpha\beta+}}}\,\frac{F_-(\zeta_{\alpha\beta+})}{F_-(-s_h)}\,\frac{\alpha(\zeta_{\alpha\beta+})}{\sqrt{t^2-s_a^2r^2}}\Bigg]\\
&\times [H(t-t_{\alpha0}) - H(t-s_ar)]\Bigg\},
\end{aligned}$$

$$\psi_\delta(x,y,t) = \frac{e_{15}C_f}{\pi\epsilon_{11}}\left\{\mathrm{Re}\left[\frac{(s+s_h)\sqrt{s_a+s_h}}{\tilde{c}_{44}(\alpha(\zeta_{\beta+})-\tilde{k}_e^2\beta(\zeta_{\beta+}))(\zeta_{\beta+}+s_h)(s_{bg}+s_h)(s'_{bg}+s_h)}\right.\right.$$
$$\left.\left.\times\frac{(s_{bg}-\zeta_{\beta+})(s'_{bg}-\zeta_{\beta+})}{(s-\zeta_{\beta+})\sqrt{s_a-\zeta_{\beta+}}}\frac{F_-(\zeta_{\beta+})}{F_-(-s_h)}\frac{\beta(\zeta_{\beta+})}{\sqrt{t^2-s_\ell^2r^2}}\right]H(t-s_\ell r)\right\},$$

$$w'_\delta(x,y,t) = \frac{1}{\pi}\left\{\mathrm{Re}\left[\frac{(s+s_h)\sqrt{s_a+s_h}}{\tilde{c}'_{44}(\alpha'(\zeta_{\alpha'+})-\tilde{k}_e'^2\beta'(\zeta_{\alpha'+}))(\zeta_{\alpha'+}+s_h)(s_{bg}+s_h)(s'_{bg}+s_h)}\right.\right.$$
$$\left.\times\frac{(s_{bg}-\zeta_{\alpha'+})(s'_{bg}-\zeta_{\alpha'+})}{(s-\zeta_{\alpha'+})\sqrt{s_a-\zeta_{\alpha'+}}}\frac{F_-(\zeta_{\alpha'+})}{F_-(-s_h)}\frac{\alpha'(\zeta_{\alpha'+})}{\sqrt{t^2-s_a'^2r^2}}\right]H(t-s'_a r)$$
$$-\mathrm{Im}\left[\frac{(s+s_h)\sqrt{s_a+s_h}}{\tilde{c}'_{44}(\alpha'(\zeta_{\alpha'\beta'+})-\tilde{k}_e'^2\beta'(\zeta_{\alpha'\beta'+}))(\zeta_{\alpha'\beta'+}+s_h)(s_{bg}+s_h)(s'_{bg}+s_h)}\right.$$
$$\left.\times\frac{(s_{bg}-\zeta_{\alpha'\beta'+})(s'_{bg}-\zeta_{\alpha'\beta'+})}{(s-\zeta_{\alpha'\beta'+})\sqrt{s_a-\zeta_{\alpha'\beta'+}}}\frac{F_-(\zeta_{\alpha'\beta'+})}{F_-(-s_h)}\frac{\alpha'(\zeta_{\alpha'\beta'+})}{\sqrt{t^2-s_a'^2r^2}}\right]$$
$$\left.\times[H(t-t_{\alpha'0})-H(t-s'_a r)]\right\},$$

$$\psi'_\delta(x,y,t) = \frac{e'_{15}C'_f}{\pi\epsilon'_{11}}\left\{\mathrm{Re}\left[\frac{(s+s_h)\sqrt{s_a+s_h}}{\tilde{c}_{44}(\alpha'(\zeta_{\beta'+})-\tilde{k}_e'^2\beta'(\zeta_{\beta'+}))(\zeta_{\beta'+}+s_h)(s_{bg}+s_h)}\right.\right.$$
$$\left.\left.\times\frac{(s_{bg}-\zeta_{\beta'+})(s'_{bg}-\zeta_{\beta'+})}{(s'_{bg}+s_h)(s-\zeta_{\beta'+})\sqrt{s_a-\zeta_{\beta'+}}}\frac{F_-(\zeta_{\beta'+})}{F_-(-s_h)}\frac{\beta'(\zeta_{\beta'+})}{\sqrt{t^2-s_\ell'^2r^2}}\right]H(t-s'_\ell r)\right\},$$

where $t_{\alpha 0}=\sqrt{s_a^2-s_\ell^2}y+s_\ell x$ and $t_{\alpha' 0}=-\sqrt{s_a'^2-s_\ell^2}y+s_\ell x$.

In acoustic and electromagnetic diffraction theories, the simple pole that represents the incident source determines the geometrical reflection/refraction fields. These geometrical scattering patterns induced by acoustic excitation depend on the incident angle of the acoustic wave, because the position of the simple pole depends on this angle. Figures 2 and 3 show that there are two different positions of the simple pole, $\zeta=-s_h=-s_a\cos\theta_a$; and the positions of $-s_h$ in the ζ-plane will directly affect the outcome of reflection/refraction fields. There are three cases, as follows.

Case (1): $s_a\cos\theta_a > s'_\ell$. In this case, the pole always lies to the right of Γ_α and $\Gamma_{\alpha'}$ but to the left of Γ_β and $\Gamma_{\beta'}$. Thus, there are pole contributions to Γ_α and $\Gamma_{\alpha'}$, but not to Γ_β and $\Gamma_{\beta'}$. After evaluating the residues of the poles for the corresponding integrals, we have

$$w_r(x,y,t) = \begin{cases} -\mathrm{Re}\left(\dfrac{\sigma_0}{\tilde{c}_{44}[s_a\sin\theta_a-\tilde{k}_e^2\sqrt{s_\ell^2-s_a^2\cos^2\theta_a}]}\right) & \\ \quad\times G(t-s_a[x\cos\theta_a+y\sin\theta_a]) & \\ \quad+\mathrm{Im}\left(\dfrac{\sigma_0}{\tilde{c}_{44}[s_a\sin\theta_a-\tilde{k}_e^2\sqrt{s_\ell^2-s_a^2\cos^2\theta_a}]}\right) & \\ \quad\times\mathcal{H}\{G(t-s_a[x\cos\theta_a+y\sin\theta_a])\}, & 0\leqslant\theta<\theta_a; \\ 0, & \theta_a\leqslant\theta<\pi; \end{cases} \tag{4.1}$$

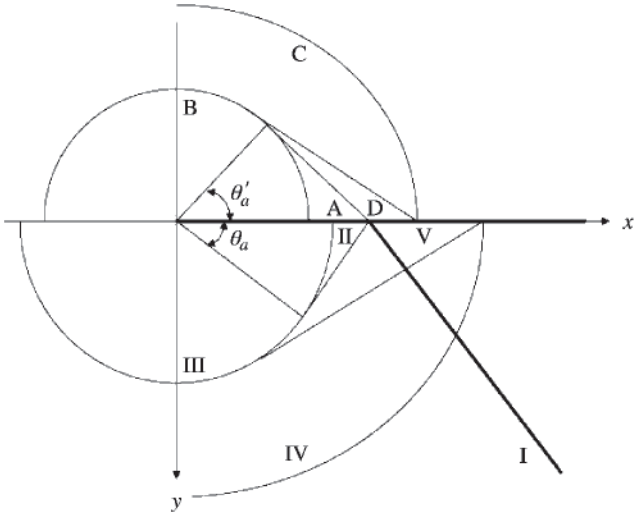

Fig. 4 The scattering patterns excited by an acoustic source: case (1). I: Incident acoustic wave; II: Reflected acoustic wave; III: Scattered acoustic wave; IV: Scattered electric wave; V: Electro-acoustic head wave; A: Refracted acoustic wave; B: Scattered acoustic wave; C: Scattered electric wave; D: Electro-acoustic head wave

$$w_r'(x,y,t) = \begin{cases} -w_r^{\prime(t)}(x,y,t), & 0 > \theta \geqslant -\theta_a'; \\ 0, & -\theta_a' > \theta \geqslant -\pi; \end{cases} \tag{4.2}$$

$$\psi_r(x,y,t) = 0, \ \ 0 \leqslant \theta < \pi; \tag{4.3}$$

$$\psi_r'(x,y,t) = 0, \ \ 0 > \theta \geqslant -\pi. \tag{4.4}$$

The complete scattering pattern is shown in Fig. 4.

Case (2): $s_\ell' \geqslant s_a \cos\theta_a > s_\ell$. In this case, the pole always lies to the right of Γ_α, $\Gamma_{\alpha'}$ and $\Gamma_{\beta'}$ but to the left of Γ_β. This means that there are pole contributions to the paths Γ_α, $\Gamma_{\alpha'}$ and $\Gamma_{\beta'}$, but not to Γ_β. After evaluating the residues of the poles for the corresponding integrals, we find that w_r is given by (4.1), w_r' is given by (4.2), ψ_r is given by (4.3) and

$$\psi_r'(x,y,t) = \begin{cases} -\psi_r^{\prime(t)}(x,y,t), & 0 > \theta \geqslant -\theta_\ell'; \\ 0, & -\theta_\ell' > \theta \geqslant -\pi. \end{cases} \tag{4.5}$$

The complete scattering pattern is shown in Fig. 5.

Case (3): $s_\ell \geqslant s_a \cos\theta_a$. In this case, the pole lies to the right of all the paths, and so, after evaluating the residues of the poles for all the corresponding integrals, we have

$$w_r(x,y,t) = \begin{cases} -\dfrac{\sigma_0 G(t - s_a[x\cos\theta_a + y\sin\theta_a])}{\tilde{c}_{44}[s_a\sin\theta_a - \tilde{k}_e^2 s_\ell \sin\theta_\ell]}, & 0 \leqslant \theta < \theta_a; \\ 0, & \theta_a \leqslant \theta < \pi; \end{cases} \tag{4.6}$$

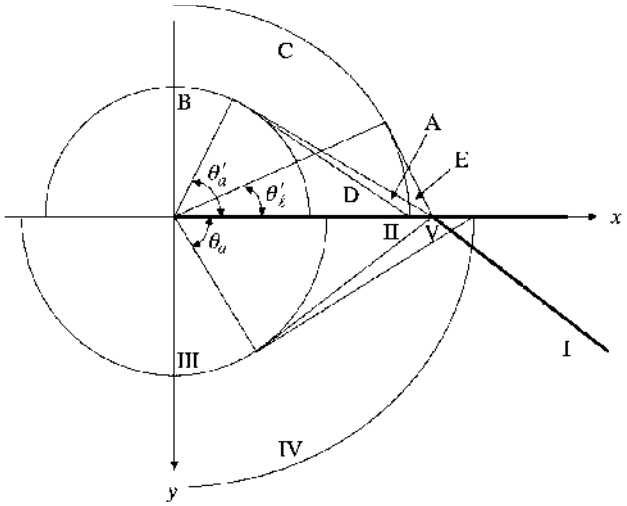

Fig. 5 The scattering patterns excited by an acoustic source: case (2). I: Incident acoustic wave; II: Reflected acoustic wave; III: Scattered acoustic wave; IV: Scattered electric wave; V: Electro-acoustic head wave; A: Refracted acoustic wave; B: Scattered acoustic wave; C: Scattered electric wave; D: Electro-acoustic head wave; E: Refracted electric wave

$$\psi_r(x, y, t) = \begin{cases} \dfrac{k_e^2 \sigma_0 G(t - s_\ell[x\cos\theta_\ell + y\sin\theta_\ell])}{e_{15}[s_a \sin\theta_a - \tilde{k}_e^2 s_\ell \sin\theta_\ell]}, & 0 \leqslant \theta < \theta_\ell; \\ 0, & \theta_\ell \leqslant \theta < \pi; \end{cases} \tag{4.7}$$

w_r' is given by (4.2) and ψ_r' is given by (4.5). The scattering pattern is shown in Fig. 6.

Next, consider the relection/refraction fields due to an incident pseudo-electric source. As shown in Fig. 7, the simple pole at $\zeta = -s_h = -s_\ell \cos\theta_\ell$ always lies to the right of all the integration paths, and thus the residue of the pole due to the corresponding integral needs to be evaluated. We find that w_r is given by (4.6), w_r' is given by (4.2), ψ_r is given by (4.7) and ψ_r' is given by (4.5). The complete scattering pattern is shown in Fig. 8.

5. Discussions

With the analytical expressions of the diffracted waves, the displacement time history at a fixed point can be traced and calculated during the electro-acoustic scattering due to the presence of a conducting crack so that we may be able to compare them with the measurements obtained in the non-destructive testing. Figures 9 and 10 show the displacement time histories at various θ with fixed y in the upper half-space due to an impulsive incident acoustic source and an electric source, respectively, with Fig. 9 corresponding to an acoustic source (case (1)). Recall that θ is measured clockwise beginning from the x-axis, so that with y fixed, $\theta = -90°$ in both figures is closest to the crack tip while $\theta = -10°$ is the farthest. A distinctive feature of scattering by a conducting crack is the ability of the head wave to tunnel through the crack, a phenomenon which is not observed in the purely elastic case (**16**). Note in Figs 9 and 10 that the head wave arrives at almost identical

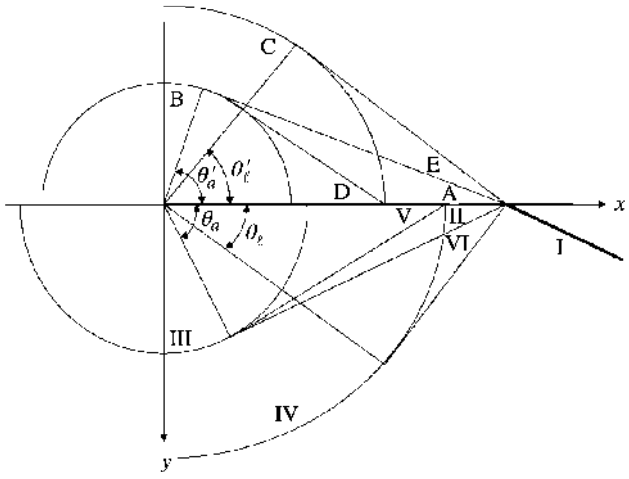

Fig. 6 The scattering patterns excited by an acoustic source: case (3). I: Incident acoustic wave; II: Reflected acoustic wave; III: Scattered acoustic wave; IV: Scattered electric wave; V: Electro-acoustic head wave; VI: Reflected electric wave; A: Refracted acoustic wave; B: Scattered acoustic wave; C: Scattered electric wave; D: Electro-acoustic head wave; E: Refracted electric wave

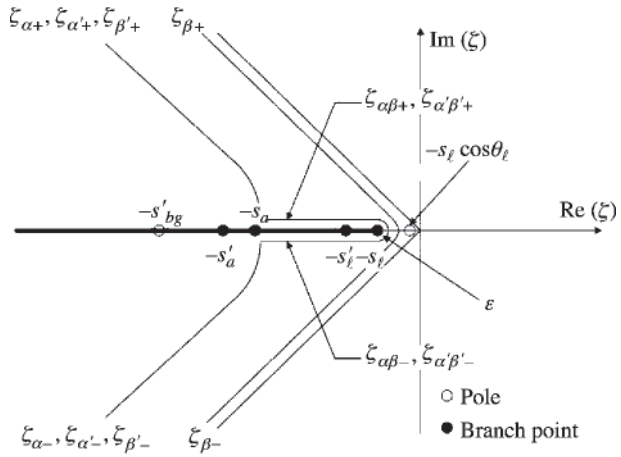

Fig. 7 Cagniard–de Hoop inversion paths for pseudo-electric excitation

times at each θ in both figures. Since the speed of light is much larger than the acoustic wave speed, the head-wave front is almost parallel to the crack. (Imagine the arc next to C in Figs 4 to 8 is much larger than the electro-acoustic head-wave line connecting the arc would be more parallel to the crack.) This electromagnetic acoustic head wave has also been observed in experiments (**20**). Another distinctive feature, which is identical to the purely elastic case, is the cancellation of the

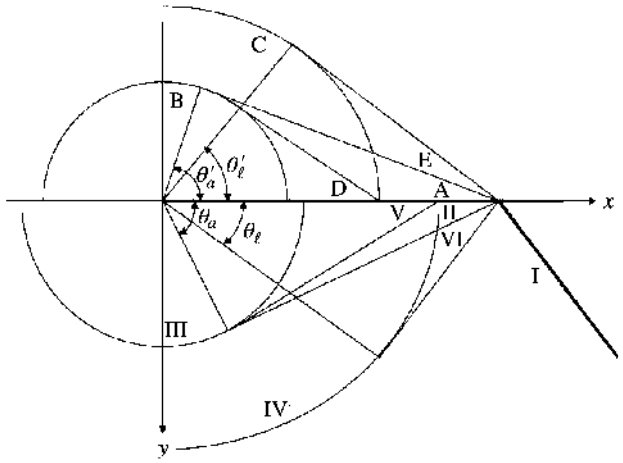

Fig. 8 The scattering patterns excited by an electric source. I: Incident acoustic wave; II: Reflected acoustic wave; III: Scattered acoustic wave; IV: Scattered electric wave; V: Electro-acoustic head wave; VI: Reflected electric wave; A: Refracted acoustic wave; B: Scattered acoustic wave; C: Scattered electric wave; D: Electro-acoustic head wave; E: Refracted electric wave

refracted acoustic wave by the transmitted acoustic wave as seen in equations (4.2), and thus, no diffracted acoustic wave or transmitted acoustic wave exists in the displacement time histories for $|\theta| < |\theta_a'|$. Also, the scattered acoustic wave originating from the crack tip can be observed in both time histories as decreasing in magnitude as the observation point is moving further away from the crack tip.

At the tail of the screen or crack, the scattered fields will become singular. In what follows, the intensity factors of the singular fields generated by the antisymmetric solutions are derived. Define

$$K_\sigma(t) = \lim_{x\to 0^-} \sqrt{2\pi|x|}\sigma_{yz}^{(s)}(x,0,t),\ \ K_{\sigma'}(t) = \lim_{x\to 0^-} \sqrt{2\pi|x|}\sigma_{yz}^{\prime(s)}(x,0,t),$$
$$K_D(t) = \lim_{x\to 0^-} \sqrt{2\pi|x|}D_y^{(s)}(x,0,t),\ \ K_{D'}(t) = \lim_{x\to 0^-} \sqrt{2\pi|x|}D_y^{\prime(s)}(x,0,t),$$

where the subscripts σ, σ', D and D' indicate stress and electric displacements for the respective lower and upper piezoelectric half-spaces.

Considering the asymptotic relations (**21**),

$$\lim_{x\to 0^-} \left(\pi|x|\right)^{1/2}\sigma_{yz}^*(x,0,p) = \lim_{\zeta\to-\infty} |p\zeta|^{1/2}p^{-1}\Sigma_-(\zeta,p),$$
$$\lim_{x\to 0^-} \left(\pi|x|\right)^{1/2}D_y^*(x,0,p) = \lim_{\zeta\to-\infty} |p\zeta|^{1/2}\hat{D}_y^*(\zeta,p),$$

one can derive that

$$K_\sigma^*(p) = K_{\sigma'}^*(p) = -\sqrt{2}\frac{g^*(p)}{\sqrt{p}}\frac{\sigma_0(s+s_h)\sqrt{s_a+s_h}}{F_-(-s_h)(s_{bg}+s_h)(s_{bg}'+s_h)}.$$

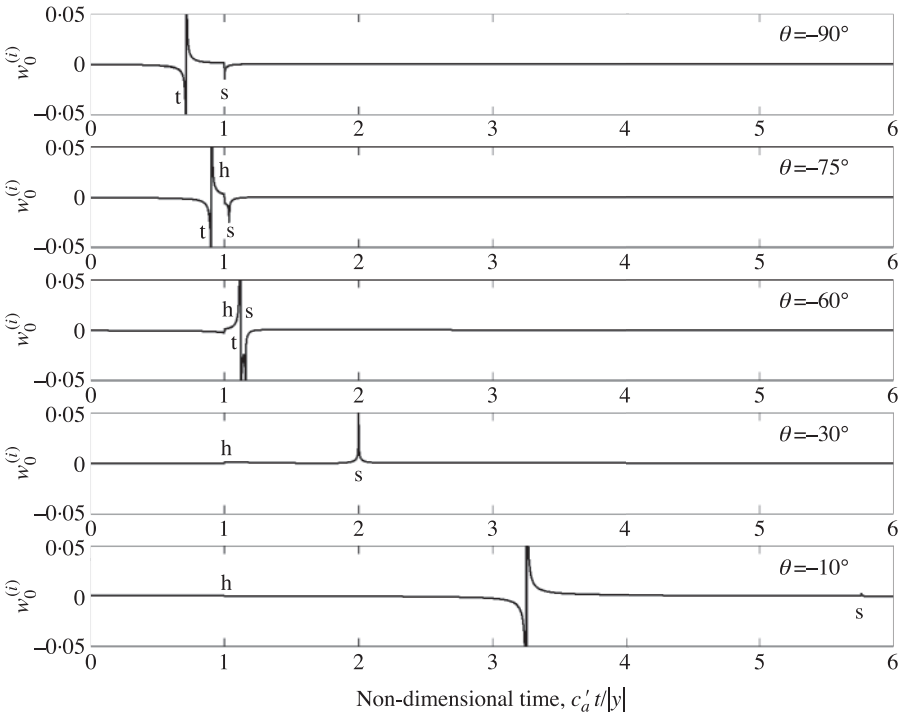

Fig. 9 Displacement time histories at various θ with fixed y due to an impulsive acoustic source incident at $\theta_a = 45°$. Labels: t = transmitted wave, h = head wave and s = scattered wave

After performing the inverse Laplace transform, one obtains

$$K_\sigma(t) = K_{\sigma'}(t) = -\frac{(s+s_h)\sqrt{s_a+s_h}}{F_-(-s_h)(s_{bg}+s_h)(s'_{bg}+s_h)}[\mathrm{Re}(\sigma_0)\chi(t) - \mathrm{Im}(\sigma_0)\mathcal{H}\{\chi(t)\}],$$

where

$$\chi(t) = \sqrt{\frac{2}{\pi}}\int_0^t \frac{1}{\sqrt{\tau}} g(t-\tau)\,d\tau.$$

Similarly, based on the definition,

$$D_y^*(\zeta, p) = [-e_{15}(1-C_f)\alpha(\zeta)A(\zeta) + \epsilon_{11}\beta(\zeta)B(\zeta)]/p,$$
$$D_y'^*(\zeta, p) = [-e'_{15}(1-C'_f)\alpha'(\zeta)A'(\zeta) + \epsilon'_{11}\beta'(\zeta)B'(\zeta)]/p.$$

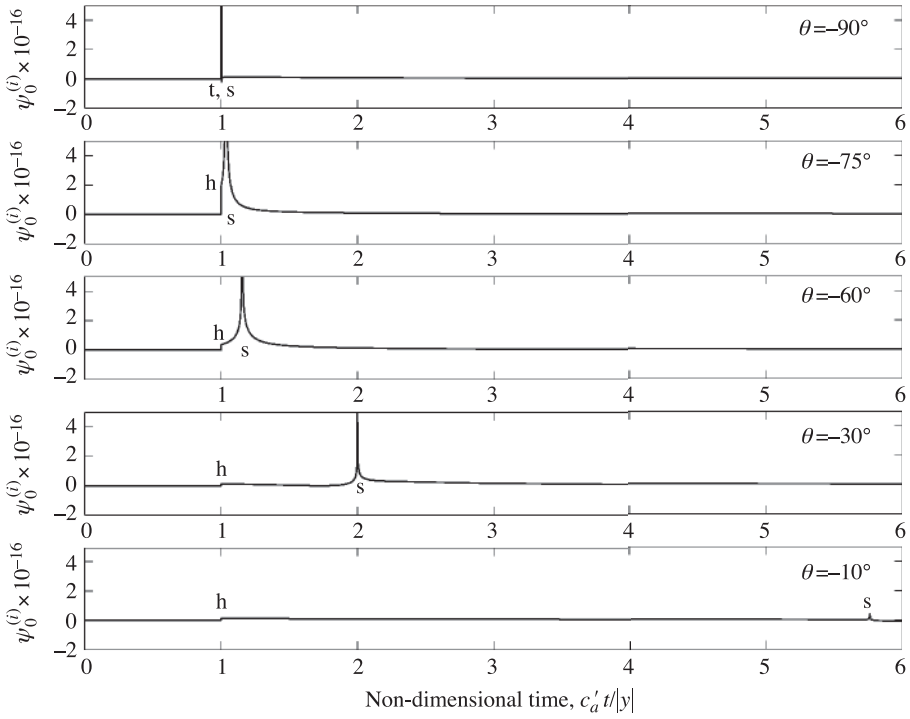

Fig. 10 Displacement time histories at various θ with fixed y due to an impulsive electric source incident at $\theta_\ell = 45°$. Labels: t = transmitted wave, h = head wave and s = scattered wave

One can then show that

$$K_D(t) = -\frac{e_{15}(s+s_h)\sqrt{s_a+s_h}\,[\mathrm{Re}(\sigma_0)\chi(t) - \mathrm{Im}(\sigma_0)\mathcal{H}\{\chi(t)\}]}{\tilde{c}_{44}(1-\tilde{k}_e^2)F_-(-s_h)(s_{bg}+s_h)(s'_{bg}+s_h)},$$

$$K_{D'}(t) = -\frac{e'_{15}(s+s_h)\sqrt{s_a+s_h}\,[\mathrm{Re}(\sigma_0)\chi(t) - \mathrm{Im}(\sigma_0)\mathcal{H}\{\chi(t)\}]}{\tilde{c}_{44}(1-\tilde{k}_e'^2)F_-(-s_h)(s_{bg}+s_h)(s'_{bg}+s_h)}.$$

The above formulae can be put into the compact forms

$$K_\sigma(t) = K_{\sigma'}(t) = -G_w(s_h)[\mathrm{Re}(\sigma_0)\chi(t) - \mathrm{Im}(\sigma_0)\mathcal{H}\{\chi(t)\}], \tag{5.1}$$

$$K_D(t) = -\frac{e_{15}G_w(s_h)}{\tilde{c}_{44}(1-\tilde{k}_e^2)}[\mathrm{Re}(\sigma_0)\chi(t) - \mathrm{Im}(\sigma_0)\mathcal{H}\{\chi(t)\}], \tag{5.2}$$

$$K_{D'}(t) = -\frac{e'_{15}G_w(s_h)}{\tilde{c}'_{44}(1-\tilde{k}_e'^2)}[\mathrm{Re}(\sigma_0)\chi(t) - \mathrm{Im}(\sigma_0)\mathcal{H}\{\chi(t)\}], \tag{5.3}$$

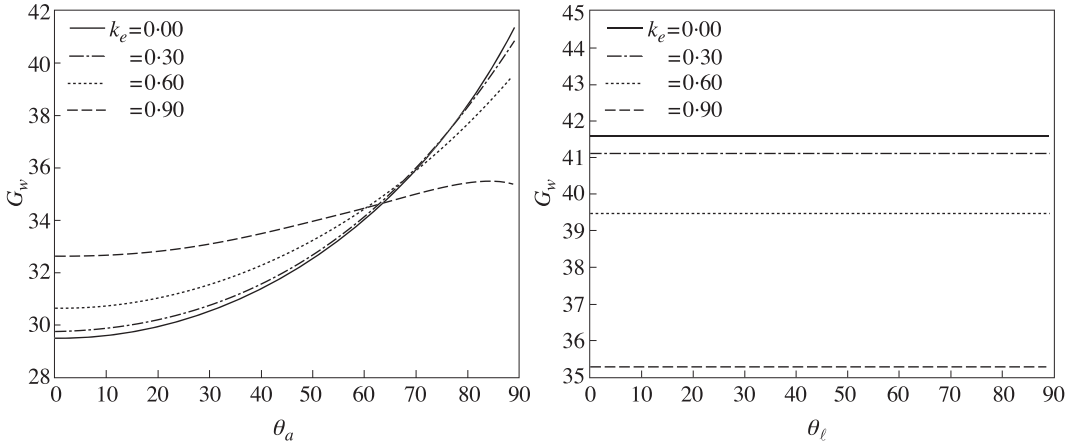

Fig. 11 Phase function G_w versus incident angle for (a) an acoustic source and (b) an electric source for various electromechanical coupling coefficients ($\tilde{k}_e$)

where

$$G_w(s_h) = \frac{(s + s_h)\sqrt{s_a + s_h}}{F_-(-s_h)(s_{bg} + s_h)(s'_{bg} + s_h)}. \tag{5.4}$$

For the first example, we consider an interface welded together by a piezoelectric lower half-space and an elastic upper half-space. The electro-mechanical coupling coefficient of the piezoelectric half-space ($\tilde{k}_e$) is allowed to increase from zero to unity while the material properties of the elastic half-space are held constant. Figure 11 displays the phase function G_w for the respective acoustic and electric excitation versus its respective incident angle for a broad range of electromechanical coefficients. Note that when $\tilde{k}_e = 0$, the problem degenerates to the case of two dissimilar purely elastic half-spaces welded together as considered in (**16**). For the acoustic incident wave case in Fig. 11(a), it is obvious that the phase function increases with increasing incident angle, where the shearing motion is more intense. The effect of the electromechanical coupling coefficient is more complicated. At small incident angle ($\cos\theta_a \approx 1$), $G_w \approx [\sqrt{2}]/[\sqrt{s_a}(1/\sqrt{1-\tilde{k}_e^4}+1)F_-(s_a)]$ while at large incident angle ($\cos\theta_a \approx 0$), $G_w \approx \sqrt{(1-\tilde{k}_e^4)/[s_a F_-(0)]}$. Usually, $F_-(\theta_a)$ is quite close to unity for any value of θ_a so that G_w decreases with increasing $\tilde{k}_e$, but this is only true for large incident angles as shown in the figure, and thus the function $F_-(\theta_a)$ is also important in the behaviour of G_w for the incident acoustic wave. On the other hand, for an incident electric wave, the horizontal slowness s_h is always close to zero for any given incident angle so that G_w is flat for each $\tilde{k}_e$ as in Fig. 11(b). Also $G_w \approx (s\sqrt{s_a})/(s_{bg}s'_{bg}) \approx (s\sqrt{1-\tilde{k}_e^4})/(\sqrt{s_a}s'_{bg})$ decreases with increasing $\tilde{k}_e$ as in Fig. 11(b). These results indicate that the competition between the Bleustein–Gulyaev wave and the shear wave dictates the behaviour of the phase function for different electromechanical coefficients.

For the second example, we consider a piezoelectric half-space with $\tilde{k}'_e = 0$ overlying another

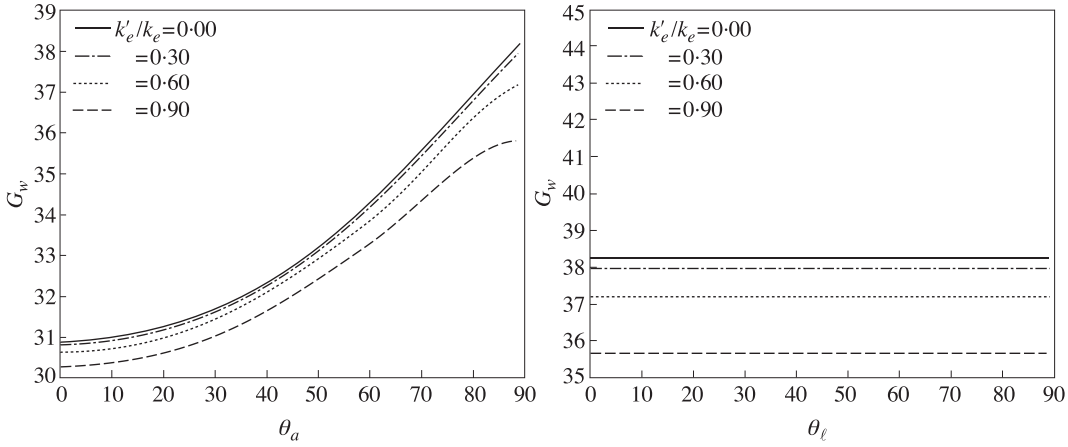

Fig. 12 Phase function G_w versus incident angle for (a) an acoustic source and (b) an electric source for various electromechanical coupling ratios ($\tilde{k}'_e/\tilde{k}_e$)

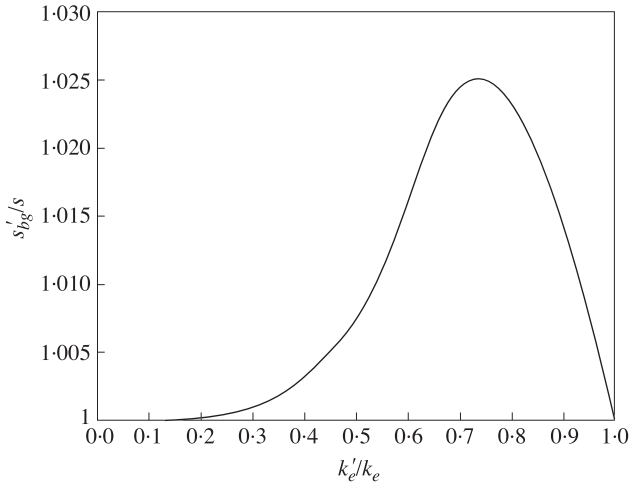

Fig. 13 Variations of slowness ratio (s'_{bg}/s) versus electromechanical coupling ratio ($\tilde{k}'_e/\tilde{k}_e$)

with $\tilde{k}_e = 0{\cdot}7$; the electromechanical coupling coefficient $\tilde{k}'_e$ of the upper purely elastic half-space is allowed to increase while the material properties of the lower piezoelectric half-space are held constant. Figure 12 displays the phase function G_w for the respective acoustic and electric excitation versus its respective incident angle for a broad range of electromechanical ratios. Like the previous example, G_w increases with increasing incident angle of the acoustic incident wave (Fig. 12(a)) while it is flat for the electric incident wave (Fig. 12(b)). Note that when the ratio $\tilde{k}'_e/\tilde{k}_e = 0$, the Maerfeld–Tournois (MT) wave does not exist, but as the ratio $\tilde{k}'_e/\tilde{k}_e$ increases to 0·62, the MT wave begins to appear. Figure 13 shows the variation of s'_{bg}/s versus $\tilde{k}'_e/\tilde{k}_e$, where $s = s_{mt}$ if the MT

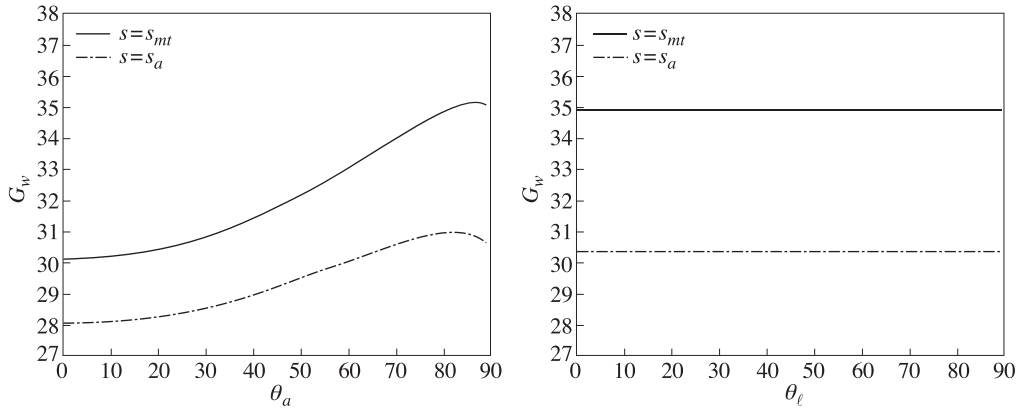

Fig. 14 Phase function G_w versus incident angle for (a) an acoustic source and (b) an electric source when Maerfeld–Tournois wave exists (solid line) and when it does not exist (dashed line)

wave exists and $s = s'_a$ otherwise. Note that in Fig. 13, $s \leqslant s'_{bg}$. Since the horizontal slowness s_h does not depend on the electromechanical coupling ratio, $G_w \approx (s + s_h)/(s'_{bg} + s_h)$ assuming that $F_-(-s_h) \approx 1$, the effect of s dominates, and the overall effect is for the phase function G_w to decrease for both the incident acoustic and the electric waves.

To examine the effect of the existence of the MT wave on the phase function G_w, we consider an interfacial crack between two identically and oppositely poled piezoelectric half-spaces. When the upper and lower half-spaces have opposite polarity ($e'_{15} = -e_{15}$), the MT wave always exists, but when they have the same polarity, the MT wave does not exist while the electromechanical coupling coefficients are identical for the two cases. Figure 14 plots these two situations for an incident acoustic and electric wave, and the phase functions are larger when the MT wave exists. This can be explained from the fact that the MT wave slowness is always higher than the shear wave slowness, and thus G_w is always higher.

Acknowledgements

This research is partially supported by a Jane Lewis Fellowship from the University of California, Berkeley (ACT), NSF grant CMS-0239130 (SL) and NSF grant CMS-9908218(SDG). This support is gratefully acknowledged.

References

1. F. Narita and Y. Shindo, Layered piezoelectric medium with interface crack under anti-plane shear, *Theor. Appl. Fract. Mech.* **30** (1998) 119–126.
2. F. Narita and Y. Shindo, Dynamic anti-plane shear of a cracked piezoelectric ceramic, *ibid.* **29** (1998) 169–180.
3. S. Li, Transient wave propagation in a transversely isotropic piezoelectric half space, *Z. Angew. Math. Phys.* **51** (2000) 236–266.

4. S. Li, On diffraction in a piezoelectric medium by half-plane: The Sommerfeld problem, *ibid.* **52** (2001) 101–134.
5. C. H. Daros, A fundamental solution for transversely isotropic, piezolectric solids under electrically irrotaional approximation, *Mech. Res. Comm.* **29** (2002) 61–71.
6. C. H. Daros, On modelling Bleustein–Gulyaev waves in non-homogeneous, transversely isotropic, piezoelectric media via stress equations of motion, *Acta Mech.* **163** (2003) 121–126.
7. S. R. Winzer, N. Shankar and A. P. Ritter, Designing confired multilayer electrostrictive actuators for reliability, *J. Amer. Ceramic Soc.* **72** (1989) 2246–2257.
8. A. Furuta and K. Uchino, Dynamic observation of crack propagation in piezoelectric multilayer actuators, *ibid.* **76** (1993) 1615–1617.
9. C. Q. Ru, X. Mao and M. Epstein, Electric-field induced interfacial cracking in multilayer electrostrictive actuators, *J. Mech. Phys. Solids* **46** (1998) 1301–1318.
10. S. Li, The electromagneto-acoustic surface wave in a piezoelectric medium: The Bleustein–Gulyaev mode, *J. Appl. Phys.* **80** (1996) 5264–5269.
11. K. Aki and P. G. Richards, *Quantitative Seismology*, 2nd edn (University Science Books, Sausalito 2000).
12. J. L. Bleustein, A new surface wave in piezoelectric materials, *Appl. Phys. Lett.* **13** (1968) 412–413.
13. Y. V. Gulyaev, Electroacoustic surface waves in solids, *Sov. Phys. JETP* **9** (1969) 37–38.
14. S. Li and P. A. Mataga, Dynamic crack propagation in piezoelectric materials, part I: electrode solution, *J. Mech. Phys. Solids* **44** (1996) 1799–1830.
15. C. Maerfeld and P. Tournois, Pure shear elastic surface wave guided by the interface of two semi-infinite media, *Appl. Phys. Lett.* **19** (1971) 117.
16. L. M. Brock and J. D. Achenbach, Extension of an interface flaw under the influence of transient waves, *Int. J. Solids Structures* **9** (1973) 53–68.
17. B. Noble, *Methods Based on the Wiener–Hopf Technique* (Pergamon Press, New York 1958).
18. L. Cagniard, *Reflection and Refraction of Progressive Seismic Waves* (McGraw–Hill, New York 1962).
19. A. T. de Hoop, A modification of Cagniard's method for solving seismic pulse problems, *Appl. Sci. Res.* B **8** (1960) 349–360.
20. Y. Liu, C. H. Wang and C. F. Ying, Electromagnetic acoustic head waves in piezoelectric media, *J. Appl. Phys.* **55** (1989) 434–436.
21. L. B. Freund, *Dynamic Fracture Mechanics* (Cambridge University Press, Cambridge 1990).

APPENDIX

Reflection and transmission coefficients

The reflection and transmission coefficients for an incident acoustic plane wave are

$$R_{aa} = \frac{\tilde{c}_{44}(s_a \sin(\theta_a) + \tilde{k}_e^2 s_\ell \sin(\theta_\ell)) - \tilde{c}'_{44}(s'_a \sin(\theta'_a) - \tilde{k}_e'^2 s'_\ell \sin(\theta'_\ell))}{\tilde{c}_{44}(s_a \sin(\theta_a) - \tilde{k}_e^2 s_\ell \sin(\theta_\ell)) + \tilde{c}'_{44}(s'_a \sin(\theta'_a) - \tilde{k}_e'^2 s'_\ell \sin(\theta'_\ell))},$$

$$T_{aa} = \frac{2\tilde{c}_{44} s_a \sin(\theta_a)}{\tilde{c}_{44}(s_a \sin(\theta_a) - \tilde{k}_e^2 s_\ell \sin(\theta_\ell)) + \tilde{c}'_{44}(s'_a \sin(\theta'_a) - \tilde{k}_e'^2 s'_\ell \sin(\theta'_\ell))},$$

$R_{a\ell} = -(e_{15}C_f/\epsilon_{11})T_{aa}$ and $T_{a\ell} = -(e'_{15}C'_f/\epsilon'_{11})T_{aa}$. The reflection and transmission coefficients for an incident pseudo-electric plane wave are

$$R_{\ell\ell} = -\frac{\tilde{c}_{44}(s_a \sin(\theta_a) + \tilde{k}_e^2 s_\ell \sin(\theta_\ell)) + \tilde{c}'_{44}(s'_a \sin(\theta'_a) - \tilde{k}_e'^2 s'_\ell \sin(\theta'_\ell))}{\tilde{c}_{44}(s_a \sin(\theta_a) - \tilde{k}_e^2 s_\ell \sin(\theta_\ell)) + \tilde{c}'_{44}(s'_a \sin(\theta'_a) - \tilde{k}_e'^2 s'_\ell \sin(\theta'_\ell))},$$

$$T_{\ell\ell} = -\frac{2\tilde{c}'_{44} e_{15} \tilde{k}_e'^2 s_\ell \sin(\theta_\ell)}{\tilde{c}_{44} e'_{15}(s_a \sin(\theta_a) - \tilde{k}_e^2 s_\ell \sin(\theta_\ell)) + \tilde{c}'_{44}(s'_a \sin(\theta'_a) - \tilde{k}_e'^2 s'_\ell \sin(\theta'_\ell))},$$

$$R_{\ell a} = T_{\ell a} = \frac{2e_{15} s_\ell \sin(\theta_\ell)}{\tilde{c}_{44}(s_a \sin(\theta_a) - \tilde{k}_e^2 s_\ell \sin(\theta_\ell)) + \tilde{c}'_{44}(s'_a \sin(\theta'_a) - \tilde{k}_e'^2 s'_\ell \sin(\theta'_\ell))}.$$